Chemical Physics Letters 834 (2024) 140985

Contents lists available at ScienceDirect

Chemical Physics Letters

journal homepage: www.elsevier.com/locate/cplett

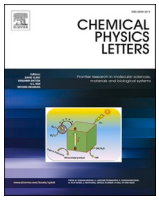

Research paper

Complexes of the noble-gas atoms with borazine: Theoretical insights into structure, stability, and bonding character

Stefano Borocci [a,b], Armando Camerlingo [a], Felice Grandinetti [a,b,*], Maria Rutigliano [c], Nico Sanna [a,c]

[a] Dipartimento per la Innovazione nei sistemi Biologici, Agroalimentari e Forestali (DIBAF), Università della Tuscia, L.go dell'Università, s.n.c., 01100 Viterbo, Italy
[b] Istituto per i Sistemi Biologici del CNR, Via Salaria, Km 29.500, 00015 Monterotondo, RM, Italy
[c] Istituto per la Scienza e Tecnologia dei Plasmi del CNR (ISTP), Via Amendola 122/D, 70126 Bari, Italy

ARTICLE INFO

Keywords:
Borazine
Bonding analysis
Energy density
Non-covalent noble gas complexes
SAPT calculations

ABSTRACT

The complexes of He, Ne, Ar, Kr and Xe with $B_3N_3H_6$ were investigated by MP2, CCSD(T), and SAPT *ab initio* methods, and accurate procedures of bonding analysis. These systems are describable as mono-, di-, and tri-coordinated to the N atoms, their stabilities following the order N-mono < N-di < N-tri. The binding energies are within 1 or 2 kcal mol^{-1}, and the interactions are dominated by the dispersion. The results are compared with those obtained recently from a DFT study on the complexes of He, Ne, Ar, and Kr with larger BN sheets [Phys. Chem. Chem. Phys. 24 (2022) 2554–2566.].

1. Introduction

Hexagonal boron nitride (*h*BN) consists of 2D ordered sheets of covalently-bound B and N atoms, structurally analogue to the carbon sheets of graphite [1]. *h*BN plays a role in different applied fields. For example, it is a convenient lubrificant in vacuum and aerospace, and is also employed in metallurgy, electronics, hydrogen storage, polymer composites, engineering materials, and biomedical fields [2]. *h*BN can be also grown on metal supports, and the *h*BN films on metals are versatile templates for different adsorbates, including atoms, metal clusters, organic molecules, metal–organic complexes, and networks [2]. A best assay of the behavior of *h*BN and *h*BN/metal supports demands to investigate their interaction with the adsorbed species. Valuable insights in this regard are, in particular, expected from the study of the interactions occurring with the simplest noble gas (Ng) atoms. The adsorption of Ng on *h*BN was indeed already the focus of various experimental and theoretical studies [3–9], generally suggesting the occurrence of two site-specific adsorption modes, a first one referable to van der Waals type contacts, and a second one of polarization type originating from the anisotropy of the electrostatic surface potential [9]. Nevertheless, the detailed nature of these bonds, and the role of the various stabilizing components still remain only partially understood. Quite recently, the interaction of He, Ne, Ar, and Kr with a single-layer *h*BN was investigated by an accurate parameterization of an anisotropic dressed pairwise potential model (PPM) [10]. To develop the parameters involved in the PPM, the complexes of Ng with the exemplary $B_{12}N_{12}H_{12}$, $B_{27}N_{27}H_{18}$, and $B_{48}N_{48}H_{24}$ clusters were investigated by B3LYP [11,12] density functional calculations (with and without inclusion of dispersion). The study of the interaction of Ng impinging along the perpendicular to the BN sheets highlighted the existence of three binding sites, namely the hollow site (H), the site on top of a B atom (T_B), and the site on top of a N atom (T_N). The stability of these structures periodically increased when going from Ng = He to Ng = Kr. The interaction energies were also decomposed by a natural energy decomposition analysis (NEDA) [13], and the NEDA curves for the various binding components were fitted with the PPM equations. The obtained potentials were eventually employed to explore the interaction of up to five Ng atoms adsorbed on the BN sheets. Particularly relevant in the present context are the results obtained from the calculations on the benchmark systems involving a single Ng. Thus, for any Ng, the stability of the various complexes invariably decreased in the order H > T_B > T_N, and, for any structure, the major attractive contribution was the charge transfer (CT), followed by comparable or nearly comparable contributions from polarization (POL) and dispersion (DISP). This result was ascribed, in particular, to the polar nature of the B-N bonds of the sheets. Based on these findings, it becomes of interest to investigate the interaction of Ng atoms with the simplest borazine, $C_3N_3H_6$ (henceforth denoted as Bz). Various systems containing Ng and Bz or its derivatives

* Corresponding author.
E-mail address: fgrandi@unitus.it (F. Grandinetti).

https://doi.org/10.1016/j.cplett.2023.140985
Received 31 August 2023; Received in revised form 15 November 2023; Accepted 19 November 2023
Available online 21 November 2023

were already explored by theoretical calculations [14,15], and the ability of Ng to form very strong complexes with boron was also ascertained [16]. The complexes of Ne, Ar, and Kr with Bz were, in particular, recently investigated [17] at the MP2 level of theory [18]. The only explored NgBz structure was the H one, whose stability increased in the order NeBz < ArBz < KrBz. However, at variance with the Ng interacting on H site of the BN sheets [10], the EDA performed according to the scheme proposed by Lu and Chen [19], and very recently upgraded as the sobEDA method [20], unraveled the by far prevailing role of the DISP, with a very minor stabilization arising from POL and CT. This discrepancy is hardly referable to a quite different polarity of the B-N bonds of the BN sheets and of Bz. For example, the molecular electrostatic potential (MEP) [21] of $B_{30}N_{30}H_{18}$ [22] and Bz [17] are quite similar, both featuring points of minimum/maximum at around the N/B atoms, with negative/positive values of the MEP. Bz is, indeed, the typical precursor of *h*BN or *h*BN/metal films [2]. To gain further insights into the nature of the interaction of Ng atoms with BN rings, stimulated also by our continuing interest for the fundamental aspects of noble gas chemistry [23,24], we decided to revisit the complexes of Bz with Ng using the Symmetry-Adapted Perturbation Theory (SAPT) [25], and the composite method that we recently proposed [26–28] to analyze the bonding situation of Ng compounds. The obtained results essentially confirmed the picture emerging from the previous MP2 study [17]. Thus, either the nature of the bond of Ng with BN is crucially affected by the size of the sheet, or the potential employed to investigate the interaction of Ng with the *h*BN substrates [10] should be revisited. The accuracy of this potential is indeed crucial for its use in Molecular Dynamics (MD) simulations [29] able to provide reaction and energy accommodation coefficients useful in modelling applied processes [30,31] involving rare gases interacting with *h*BN. Indirect implications are also expected for the use of low-energy noble gas (Ne, Ar, Xe) ion beams to induce a structural rearrangement of *h*BN and change its electronic properties [32,33].

2. Theoretical methods

2.1. SAPT analysis

The nature of the bond occurring in the NgBz was first assayed by SAPT analysis. In SAPT [25], the total Hamiltonian H of a dimer AB is expressed as $H = F_A + F_B + V + W_A + W_B$, where F_X ($X = A,B$) is the Fock operator, V is the intermolecular interaction operator, and W_X is the Møller-Plesset fluctuation operator, in turn defined as $W_X = H_X - F_X$. The E_{int}^{SAPT} is expanded as a perturbative series, and we presently included the following terms:

$$E_{int}^{SAPT} = E_{elst}^{(10)} + E_{exch}^{(10)} + E_{ind,r}^{(20)} + E_{exch-ind,r}^{(20)} + \delta E_{int,r}^{HF} + E_{elst,r}^{(12)} + {}^{t}E_{ind}^{(22)} + {}^{t}E_{exch-ind}^{(22)} + E_{disp}^{(20)} + E_{exch-disp}^{(20)} + E_{elst,r}^{(13)} + \varepsilon_{exch}^{(1)}(CCSD) + E_{disp}^{(21)} + E_{disp}^{(22)} \quad (1)$$

the first (1/2) and the second (0/1/2/3) number superscript in parenthesis indicating the first-/second-order, and the zeroth-/first-/second-/third-order intramonomer electron correlation correction to V and W, respectively. The notations in subscript indicate the classical (Coulombic) electrostatic energy (*elst*), the exchange term (*exch*) that results from the antisymmetrization of the wave-function, the induction energy (*ind*) (intended as polarization plus charge transfer), and the dispersion energy (*disp*). The "*r*" indicates the inclusion of the coupled Hartree-Fock (HF) response for the perturbed system. The $\delta E_{int,r}^{HF}$ term collects the contributions to the supermolecular HF energy beyond the second-order of intermolecular operator, the ${}^{t}E_{ind}^{(22)}$ is the part of $E_{ind}^{(22)}$ not included in $E_{ind,r}^{(20)}$, and $\varepsilon_{exch}^{(1)}(CCSD) = E_{exch}^{(1)}(CCSD) - E_{exch}^{(10)}$ is the part of $\varepsilon_{exch}^{(1)}(\infty)$ with CCSD intra-monomer excitations.

E_{int}^{SAPT} is the sum of E_{elst}, E_{ind}, E_{disp} and E_{exch} terms obtained by the following grouping:

$$E_{elst} = E_{elst}^{(10)} + E_{elst,r}^{(12)} + E_{elst,r}^{(13)} \quad (2a)$$

$$E_{ind} = E_{ind,r}^{(20)} + E_{exch-ind,r}^{(20)} + {}^{t}E_{ind}^{(22)} + {}^{t}E_{exch-ind}^{(22)} + \delta E_{int,r}^{HF} \quad (2b)$$

$$E_{disp} = E_{disp}^{(20)} + E_{disp}^{(21)} + E_{disp}^{(22)} + E_{exch-disp}^{(20)} \quad (2c)$$

$$E_{exch} = E_{exch}^{(10)} + \varepsilon_{exch}^{(1)}(CCSD) \quad (2d)$$

Table 1
Criteria to assign the Ng-X bonds in terms of the sign of the $H(r)$ at around the BCP, and of covalency.

Assignment	$H(\boldsymbol{r})$ at around the BCP	
	Ng side	X side
A	negative	negative
B^{l} or C^{l}	positive	positive
B^{t} or C^{t}	positive	negative
	negative	positive
	negative	negative

Assignment	Covalency		
	ρ_s(ave)[a]	$H(\Omega_s)$	Notation
Cov	≥ 0.08	invariably negative	H^{-}
pCov	< 0.08	invariably negative	H^{-}
	any value	from negative to positive	$H^{+/-}$ (positive on the average)
			$H^{-/+}$ (negative on the average)
nCov	any value	invariably positive	H^{+}

[a] ea_0^{-3}.

2.2. Composite bonding analysis

The NgBz were further assayed using our recently proposed method of bonding analysis [26–28]. It relies on the study of the electron density $\rho(\boldsymbol{r})$ [34], the electron energy density $H(\boldsymbol{r})$ [26,35,36], and the reduced density gradient (RDG) $s(\boldsymbol{r})$ [37,38]. The employed step-by-step procedure [28] is briefly recalled below, and further details are given in Refs. 26-28.

Step 1. Any Ng-X bond (X = binding partner) is first ascertained by analyzing the topology of the $\rho(\boldsymbol{r})$ and locating the corresponding bond path (BP) and bond critical point (BCP) (the classical AIM analysis).

Step 2. The topology of the $H(\boldsymbol{r})$ of the whole molecule is analyzed. This typically produces various critical points (HCPs) of rank 3 and signature −3, −1, +1, or + 3. The contour lines these points belong to are collected as HCP lines, and then combined with a set of standard (STD) $H(\boldsymbol{r})$ lines (typically the patterns $\pm k \times 10^{n}$; $k = 0, 1, 2, 4, 8$; $n = -5 \div 6$).

Step 3. The HCP/STD lines are plotted as 2D or 3D graphs, whose visual inspection allows to assign the bond as of type A, B, or C. As best discussed previously [26–28], the $H(\boldsymbol{r})$ generally partitions the atomic space into a inner region of negative values, indicated as $H^{-}(\boldsymbol{r})$, and an outer region of positive values, indicated as $H^{+}(\boldsymbol{r})$. When two atoms

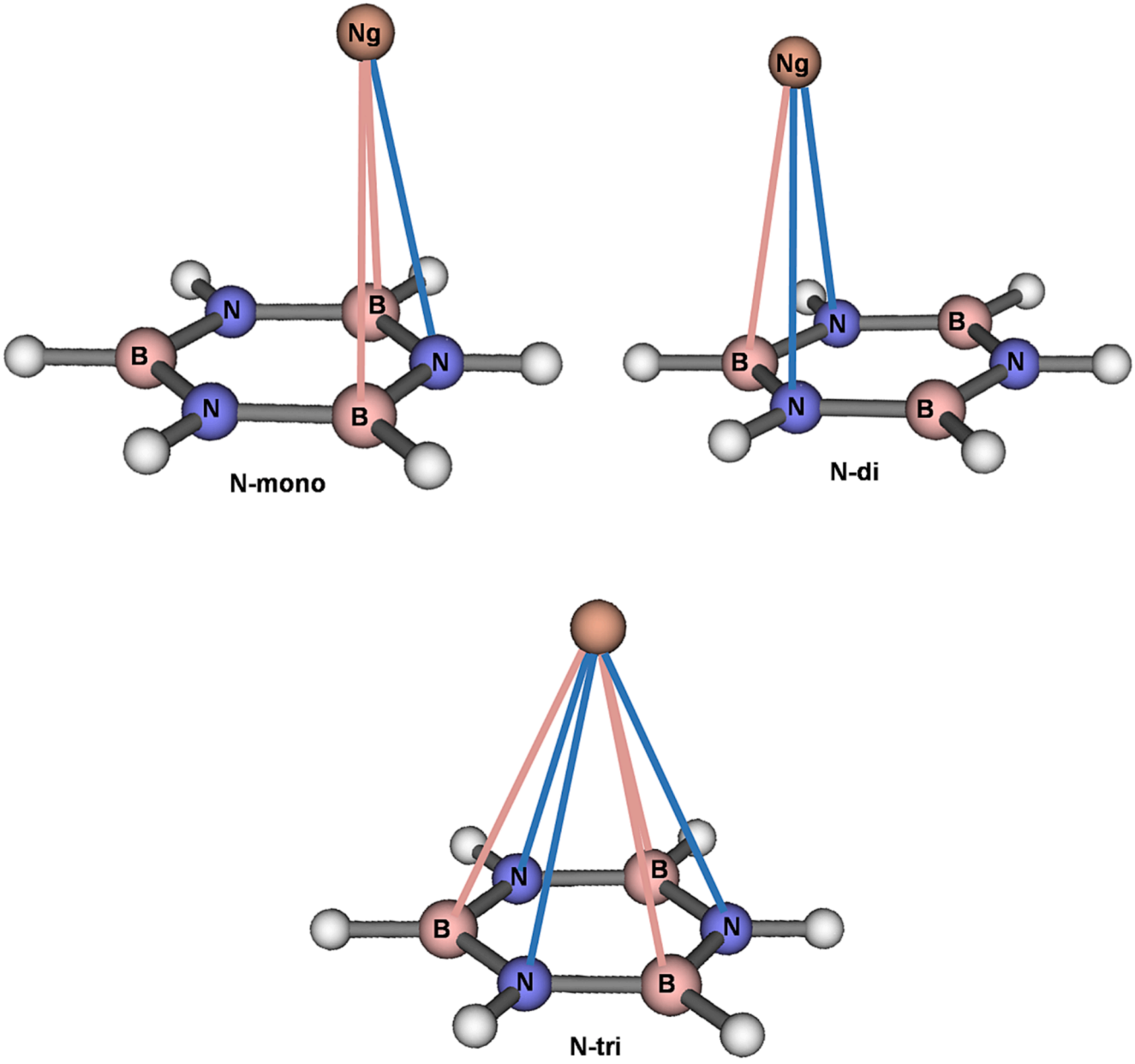

Fig. 1. Connectivities and shortest equivalent Ng-B and Ng-N bonds of the NgBz complexes.

form a chemical bond, these regions combine in modes that signal the nature of the interaction. Particularly for the Ng-X, it is possible to recognize three major situations. In *interactions of type A*, the atoms overlap all the contour lines of their outer $H^{+}(\boldsymbol{r})$ regions, and part of the contour lines of their inner $H^{-}(\boldsymbol{r})$ regions, the bond appearing as a continuous region of negative values of $H(\boldsymbol{r})$, plunged in a zone of positive values. The bond is topologically-signed by a (3,+1) HCP falling on the bond axis. Typical examples are covalent bonds, or donor–acceptor interactions with some degree of electron sharing. In *interactions of type B*, the $H^{-}(\boldsymbol{r})$ region of Ng is, again, overlapped with the $H^{-}(\boldsymbol{r})$ region of the binding partner, but *i*) no HCP does exist on the bond axis, and *ii*) the Ng-X inter-nuclear region includes a region of positive $H(\boldsymbol{r})$. Typical examples are the complexes of Ng donors with strong Lewis acceptors. In *interactions of type C*, Ng and X overlap only part of their $H^{+}(\boldsymbol{r})$ regions, their $H^{-}(\boldsymbol{r})$ regions remaining perfectly closed and distinguishable, separated by a region of positive $H(\boldsymbol{r})$. Typical examples are non-covalent contacts of variable nature.

Step 4. The assignment of the bond is refined by examining the $H(\boldsymbol{r})$ along the Ng-X BP, particularly at around the BCP. This serves to confirm the interactions of type A, and to distinguish the interactions of type B and C into B-loose (B^{l}) or B-tight (B^{t}), and C-loose (C^{l}) or C-tight (C^{t}). The adopted criteria are given in Table 1.

Step 5. Interactions of type A, B^{l}/B^{t}, or C^{l}/C^{t} are then assayed in terms of covalency. This is accomplished by integrating the $\rho(\boldsymbol{r})$ and the $H(\boldsymbol{r})$ over the volume Ω_s enclosed by the $s(\boldsymbol{r})$ isosurface associated with the Ng-X BCP. The value of the $s(\boldsymbol{r})$ is chosen by examining, particularly at around the BCP, the $s(\boldsymbol{r})$ *vs* sign$(\lambda_2) \times \rho(\boldsymbol{r})$ 2D plot [λ_2 is the second eigenvalue of the Hessian matrix of $\rho(\boldsymbol{r})$, with $\lambda_1 < \lambda_2 < \lambda_3$]. The selected value is the highest one that still avoids the tails of the atomic densities, and typically ranges between 0.2 and 0.5. The average $\rho(\boldsymbol{r})$, ρ_s(ave), and the average, maximum, and minimum $H(\boldsymbol{r})$, H_s(ave/max/min) over Ω_s are, then, calculated and employed to assign the bond as covalent (Cov), partially-covalent (pCov) or non-covalent (nCov) according to the criteria given in Table 1.

Step 6. The bond is finally classified using the notations Cov(Type), pCov[Type/$H(\Omega_s)$], or nCov(Type). For example, Cov(A), pCov($B^{t}/H^{-/+}$), or nCov(C^{l}).

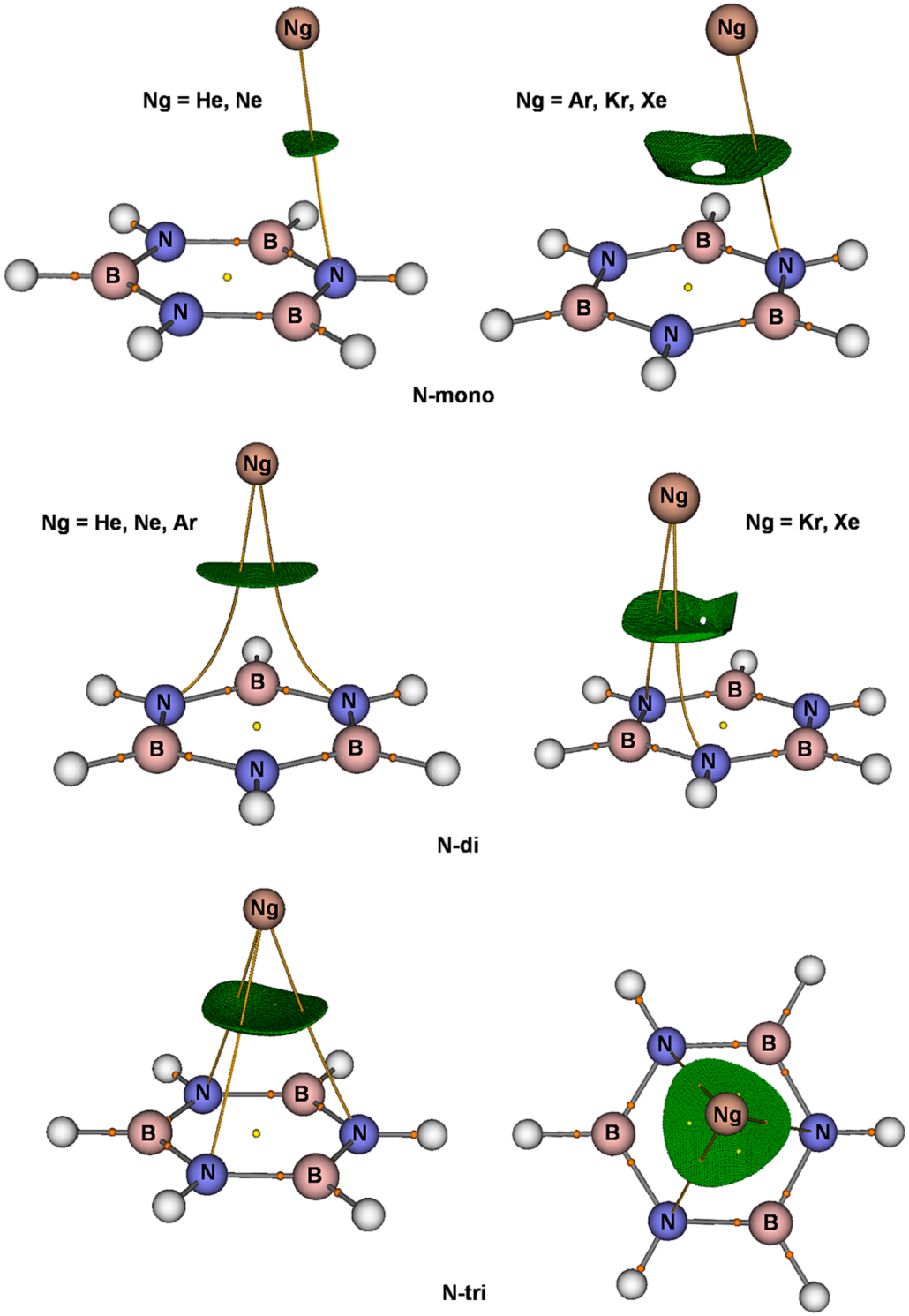

Fig. 2. MP2/aVTZ $s(\boldsymbol{r}) = 0.5$ RDG isosurfaces of the NgBz complexes. The graphs include the AIM bond paths and critical points (orange: 3,-1: yellow: 3,+1; green: 3,+3). (For interpretation of the references to colour in this figure legend, the reader is referred to the web version of this article.)

3. Computational details

The employed theoretical levels were the Møller-Plesset truncated at the second-order (MP2) [18], and the coupled cluster with inclusion of single and double substitutions, CCSD, and an estimate of connected triples, CCSD(T) [39]. The employed basis sets were the Dunning's correlation consistent aug-cc-pV*n*Z (n = D, T) (henceforth denoted as aV*n*Z) [40]. The Xe atom was treated with the aV*n*Z-PP basis set and the Stuttgart/Cologne small-core, scalar-relativistic effective core potential (ECP-28) [41]. The electronic MP2/aVTZ and CCSD(T)/aVTZ binding energies (BEs) (not including the ZPE) were corrected for the basis set superposition error (BSSE) using the counterpoise method by Boys and Bernardi [42].

Complete basis set (CBS) electronic energies were obtained by extrapolating the CCSD(T)/aVDZ and CCSD(T)/aVTZ correlation energies using the cubic formula [43]:

Table 2
MP2/aVTZ optimized distances (Å) of the shortest Ng-B and Ng-N bonds of the NgBz complexes (see Fig. 1).

	N-mono		N-di		N-tri		
	Ng-B	Ng-N	Ng-B	Ng-N	Ng-B	Ng-N	Ng-Centre[a]
He	3.6388	3.4859	3.4603	3.5968	3.5707	3.5530	3.3367
Ne	3.5696	3.4136	3.3931	3.5321	3.5710	3.5532	3.3369
Ar	3.7261	3.5770	3.5607	3.6934	3.7358	3.7189	3.5128
Kr	3.7383	3.5897	3.5713	3.7037	3.7564	3.7396	3.5347
Xe	3.8524	3.7083	3.6938	3.8219	3.8799	3.8636	3.6656

[a] Centre of the ring.

$$E^{corr}(\mathrm{CBS}) = \frac{E_3^{corr} \times 3^3 - E_2^{corr} \times 2^3}{3^3 - 2^3} \tag{3}$$

The optimized geometries and harmonic frequencies of the NgBz were obtained at the MP2/aVTZ level using the Gaussian 09 (G09, Version D1) [44].

The SAPT [25] calculations were performed with the SAPT2016 [45] using the G09 for the integrals calculation. The employed basis set, denoted here as aVDZ/mbf, combined the aVDZ with a set of extra 3*s*3*p*2*d*1*f* mid-bond functions [46] (three *s* and three *p* functions with exponents 0.9, 0.3, 0.1, two *d* functions with exponents 0.6 and 0.2, and one *f* function with exponent 0.3) placed for any NgBz at the midpoint on the perpendicular between Ng and Bz. As noted previously [46], especially for van der Waals systems of dispersive character, the addition of mbf to a moderately polarized basis set ensures a proper evaluation of the interaction energy.

The $\rho(\boldsymbol{r})$, the $H(\boldsymbol{r})$ and the $s(\boldsymbol{r})$ were calculated at the MP2/aVTZ level of theory using G09. Based on an our previous benchmark study [27], the use of the CCSD density is expected to produce only minor differences, if any. The $\rho(\boldsymbol{r})$ is defined by the equation [34]:

$$\rho(\boldsymbol{r}) = \sum_i \eta_i |\varphi_i(\boldsymbol{r})|^2 \tag{4}$$

where η_i is the occupation number of the natural orbital φ_i, in turn expanded as a linear combination of the basis functions.

The $H(\boldsymbol{r})$ [26,35,36] is the sum of the kinetic energy density $G(\boldsymbol{r})$ and the potential energy density $V(\boldsymbol{r})$. The $G(\boldsymbol{r})$ is defined by the equation [34,47]:

$$G(\boldsymbol{r}) = \frac{1}{2} \sum_{i=1}^{NO} \eta_i |\nabla \varphi_i(\boldsymbol{r})|^2 \tag{5}$$

where the sum runs over all the occupied natural orbitals φ_i of occupation numbers η_i. The $V(\boldsymbol{r})$ is evaluated [34] from the local form of the virial theorem:

$$V(\boldsymbol{r}) = \frac{1}{4}\nabla^2\rho(\boldsymbol{r}) - 2G(\boldsymbol{r}) \tag{6}$$

The $s(\boldsymbol{r})$ is defined by the equation [37,38]:

$$s(\boldsymbol{r}) = \frac{|\nabla\rho(\boldsymbol{r})|}{2(3\pi^2)^{\frac{1}{3}} \times \rho(\boldsymbol{r})^{\frac{4}{3}}} \tag{7}$$

The integration of $\rho(\boldsymbol{r})$ or $H(\boldsymbol{r})$ over the volume Ω_s enclosed by a given $s(\boldsymbol{r})$ was accomplished by producing an orthogonal grid of points that encloses the isosurface and applying the formula:

$$P(\Omega_s) = \sum_{i(\mathrm{RDG}<s)} P(\boldsymbol{r}_i) d_x d_y d_z, \tag{8}$$

where $P(\boldsymbol{r}_i)$ is the value of $\rho(\boldsymbol{r})$ or $H(\boldsymbol{r})$ at the grid point $\boldsymbol{r}_i$, and d_x, d_y, and d_z are the grid step sizes along *x*,*y*, and *z* ($d_x = d_y = d_z = 0.025\ a_0$). The summation is carried out on all grid points $\boldsymbol{r}_i$ having RDG $< s$. All the calculations were performed using $s(\boldsymbol{r}) = 0.5$.

The $\rho(\boldsymbol{r})$, the $H(\boldsymbol{r})$, and the $s(\boldsymbol{r})$ were analyzed with Multiwfn (version 3.8.dev) [19] using the wave functions stored in the wfx files generated with G09. The 3D plots of the $H(\boldsymbol{r}) = 0$ isosurfaces were as well produced with Multiwfn.

Table 4
SAPT analysis of the NgBz complexes (see Fig. 1) performed with the aVDZ/mbf basis set at the MP2/aVTZ optimized geometries. The values in parentheses are the percentage contributions of E_{elst}, E_{ind}, and E_{disp} to ($E_{elst} + E_{ind} + E_{disp}$). All values in kcal/mol.

		E_{elst}	E_{ind}	E_{disp}	E_{exch}	E_{int}^{SAPT} [a]
HeBz	N-mono	−0.043 (12.29)	−0.017 (4.86)	−0.29 (82.86)	0.21	−0.14
	N-di	−0.044 (12.19)	−0.017 (4.71)	−0.30 (83.10)	0.22	−0.14
	N-tri	−0.059 (12.80)	−0.022 (4.77)	−0.38 (82.43)	0.29	−0.17
NeBz	N-mono	−0.22 (23.73)	−0.017 (1.83)	−0.69 (74.43)	0.65	−0.28
	N-di	−0.22 (23.21)	−0.018 (1.90)	−0.71 (74.89)	0.67	−0.28
	N-tri	−0.23 (21.74)	−0.018 (1.70)	−0.81 (76.56)	0.74	−0.32
ArBz	N-mono	−0.65 (24.23)	−0.083 (3.09)	−1.95 (72.68)	1.89	−0.79
	N-di	−0.66 (24.02)	−0.088 (3.20)	−2.00 (72.78)	1.96	−0.79
	N-tri	−0.72 (23.74)	−0.093 (3.07)	−2.22 (73.19)	2.17	−0.86
KrBz	N-mono	−1.18 (28.37)	−0.16 (3.85)	−2.82 (67.79)	3.30	−0.86
	N-di	−1.22 (28.37)	−0.17 (3.95)	−2.91 (67.67)	3.44	−0.86
	N-tri	−1.31 (28.17)	−0.17 (3.66)	−3.17 (68.17)	3.73	−0.92

[a] $E_{int}^{SAPT} = E_{elst} + E_{ind} + E_{disp} + E_{exch}$.

Table 3
Binding energies (kcal/mol) of the NgBz (see Fig. 1) and Ng($B_{48}N_{48}H_{24}$).

	NgBz												$Ng(B_{48}N_{48}H_{24})$[a]		
	MP2/aVTZ[b]			CCSD(T)/aVTZ[b]			CCSD(T)/CBS			SAPT/aVDZ/mbf			B3LYP-D3/6-311G(d,p)		
	N-Mono	N-Di	N-Tri	N-Mono	N-Di	N-Tri	N-Mono	N-Di	N-Tri	N-Mono	N-Di	N-Tri	T_N	T_B	H
He	−0.11	−0.11	−0.14	−0.14	−0.14	−0.18	−0.18	−0.19	−0.23	−0.14	−0.14	−0.17	−0.27	−0.29	−0.31
Ne	−0.21	−0.22	−0.25	−0.27	−0.28	−0.32	−0.53	−0.55	−0.59	−0.28	−0.28	−0.32	−0.82	−0.91	−0.92
Ar	−0.87	−0.89	−0.98	−0.76	−0.77	−0.85	−1.11	−1.13	−1.22	−0.79	−0.79	−0.86	−1.88	−1.93	−2.01
Kr	−1.06	−1.08	−1.18	−0.84	−0.85	−0.92	−2.13	−2.15	−2.29	−0.86	−0.86	−0.92	−2.73	−2.74	−2.88
Xe	−1.33	−1.34	−1.46	−0.97	−0.98	−1.06	−2.64	−2.66	−2.82						

[a] Taken from Ref. 10.
[b] Including the BSSE.

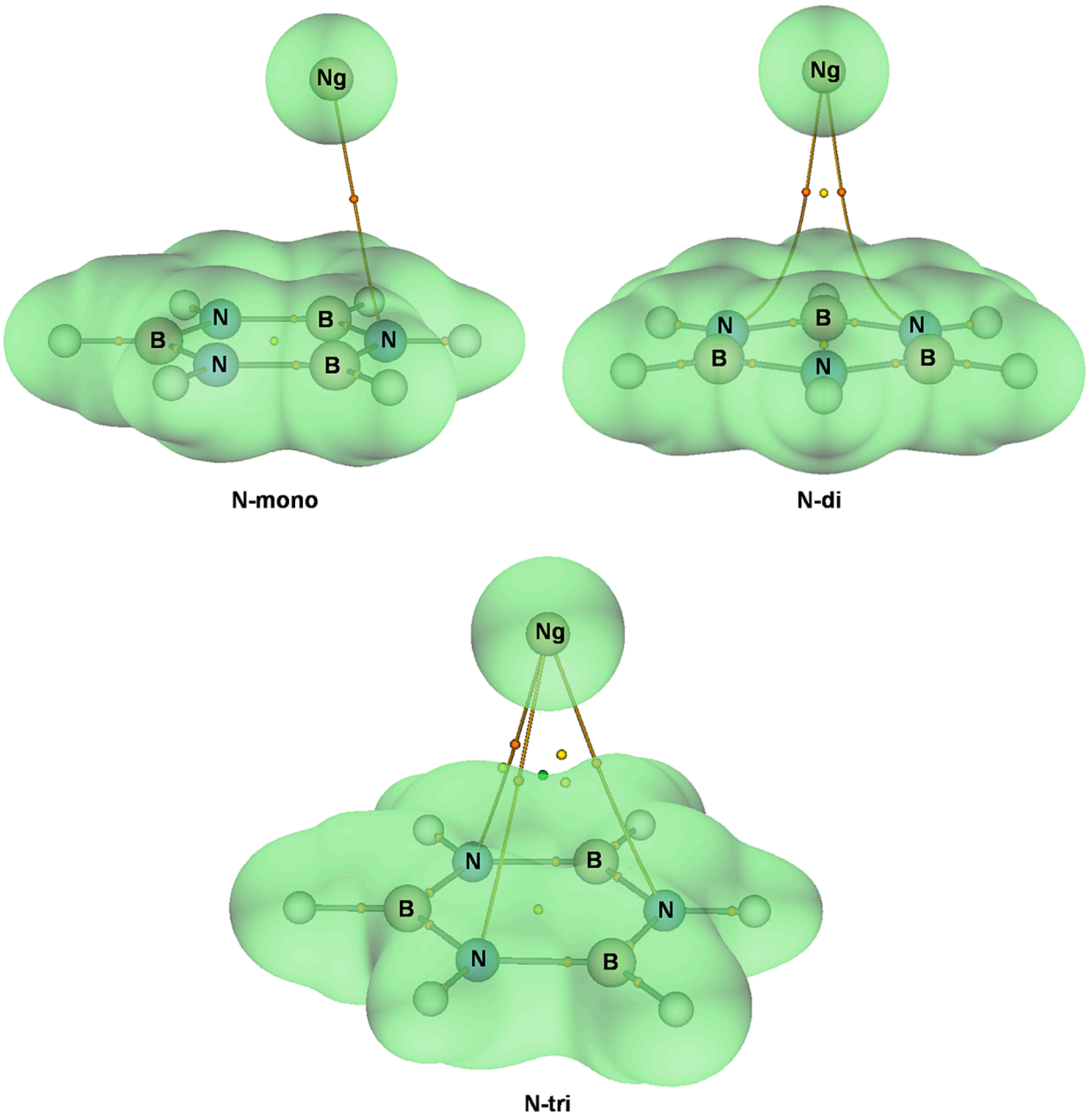

Fig. 3. MP2/aVTZ $H(\boldsymbol{r}) = 0$ isosurfaces of the NgBz complexes. The graphs include the AIM bond paths and critical points (orange: 3,-1: yellow: 3,+1; green: 3,+3). (For interpretation of the references to colour in this figure legend, the reader is referred to the web version of this article.)

4. Results and discussion

4.1. Geometries and stabilities of the NgBz

The MP2/aVTZ geometries of the NgBz (Ng = He-Xe) were obtained by optimizing the distance of a Ng impinging along the perpendicular to Bz kept frozen at its MP2/aVTZ optimized structure (B-N: 1.432 Å, B-H: 1.192 Å, N-B-N: 116.9°). Starting from different conceivable interaction sites, we located for any Ng three distinct complexes, whose connectivities are shown in Fig. 1. All these structures were characterized as true minima on the MP2/aVTZ potential energy surface (PES), the only exception being the HeBz N-di, featuring a single imaginary frequency of $11i$ cm^{-1}. The employed terminology N-mono, N-di, and N-tri actually mirrors the results of the AIM analysis. Thus, as shown in Fig. 2, the only located BCPs and BPs were those corresponding to the Ng-N bonds: a single/two equivalent/three equivalent BCP(s)/BP(s) for the N-mono/N-di/N-tri. This topology, however, does not imply the exclusive occurrence of Ng-N contacts. This emerges also by inspecting the RDG isosurfaces associated with the various BCPs, shown as well in Fig. 2. In these regions, both the electron density and its reduced gradient are small, thus signing non-covalent interactions [38,39]. The surfaces look, in particular, generally flat, and covering a rather wide region of space, suggesting interactions of Ng with both the B and the N atoms. This actually anticipates the dispersive character of the various complexes (*vide infra*).

The distances of the shortest Ng-B and Ng-N bonds of the NgBz, shown in Fig. 1, are quoted in Table 2.

Like the complexes of Ng with C_6H_6 [48] and other isoelectronic heterocyclic compounds [17], these values generally exceed the sum of the van der Waals radii of B/N and Ng. Their differences, however, are suggestive of preferential interactions of Ng with B or N. Thus, in the N-tri complexes, Ng is sitting at the centre of the ring, and the Ng-B and Ng-N distances are comparable, ranging, respectively, between *ca.* 3.57 and *ca.* 3.88 Å, and *ca.* 3.55 and *ca.* 3.86 Å. This was the only isomer reported

Table 5
MP2/aVTZ type and properties of the Ng-Bz bonds (see Fig. 1) calculated over the $s(r) = 0.5$ RDG isosurface at around the BCP. Ω_s is the volume (a_0^3) enclosed by $s(r)$, and $N(\Omega_s)$, ρ_s(ave), and H_s(ave/max/min) are, respectively, the total electronic charge (me), the average electron density ($e\ a_0^{-3}$), and the average, maximum and minimum value of $H(r)$ (hartreea_0^{-3}) over Ω_s.

	Isomer	Type	Ω_s	$N(\Omega_s)$	ρ_s(ave)	H_s(ave/max/min)	$H(\Omega_s)$	Assignment
HeBz	N-mono	C^l	0.0948	0.14	0.0015	0.000465/0.000540/0.000416	H^+	nCov(C^l)
	N-di	C^l	0.2250	0.30	0.0013	0.000446/0.000517/0.000378	H^+	nCov(C^l)
	N-tri	C^l	0.6951	0.94	0.0013	0.000466/0.000529/0.000403	H^+	nCov(C^l)
NeBz	N-mono	C^l	0.2028	0.57	0.0028	0.000613/0.000651/0.000566	H^+	nCov(C^l)
	N-di	C^l	0.4298	1.08	0.0025	0.000587/0.000624/0.000524	H^+	nCov(C^l)
	N-tri	C^l	1.0863	2.40	0.0022	0.000587/0.000645/0.000511	H^+	nCov(C^l)
ArBz	N-mono	C^l	1.3370	4.32	0.0032	0.000648/0.000991/0.000399	H^+	nCov(C^l)
	N-di	C^l	1.1193	4.24	0.0038	0.000712/0.000874/0.000590	H^+	nCov(C^l)
	N-tri	C^l	2.3749	8.09	0.0034	0.000685/0.000829/0.000540	H^+	nCov(C^l)
KrBz	N-mono	C^l	2.0305	8.14	0.0040	0.000717/0.00102/0.000464	H^+	nCov(C^l)
	N-di	C^l	2.1022	8.97	0.0043	0.000728/0.000897/0.000434	H^+	nCov(C^l)
	N-tri	C^l	3.0578	13.0	0.0043	0.000758/0.000879/0.000586	H^+	nCov(C^l)
XeBz	N-mono	C^l	3.0286	13.5	0.0044	0.000626/0.000943/0.000444	H^+	nCov(C^l)
	N-di	C^l	3.1156	14.5	0.0047	0.000624/0.000789/0.000415	H^+	nCov(C^l)
	N-tri	C^l	4.0025	18.8	0.0047	0.000655/0.000784/0.000510	H^+	nCov(C^l)

in the recent investigation [17] of the complexes of Ne, Ar, and Kr with Bz, and is the corresponding analogue of the H structure located for the complexes of He, Ne, Ar, and Kr with $B_{12}N_{12}H_{12}$, $B_{27}N_{27}H_{18}$, and $B_{48}N_{48}H_{24}$ [10]. In the N-mono complexes, the Ng-B distances (between *ca.* 3.64 and *ca.* 3.85 Å) are longer than the Ng-N ones (between *ca.* 3.49 and *ca.* 3.71 Å) by nearly 0.15 Å. On the other hand, in the N-di complexes, the Ng-B distances (between *ca.* 3.46 and *ca.* 3.69 Å) are shorter than the Ng-N ones (between *ca.* 3.60 and *ca.* 3.82 Å) by nearly 0.12–0.13 Å. The N-mono and the N-di NgBz can be, therefore, regarded, respectively, as the corresponding analogues of the T_N and T_B isomers located for the complexes of Ng with $B_{12}N_{12}H_{12}$, $B_{27}N_{27}H_{18}$, and $B_{48}N_{48}H_{24}$ [10]. These correspondences are also supported by energetic considerations. In fact, the order of stability of the NgBz isomers, namely N-mono < N-di < N-tri strictly parallels that predicted for the complexes of Ng with the larger clusters [10], namely $T_N < T_B <$ H. The relevant data are given in Table 3.

At any employed computational level, including the MP2/aVTZ, CCSD(T)/aVTZ, CCSD(T)/CBS and SAPT/aVDZ/mbf, the N-tri has the highest BE, the N-di is less stable by ca. 0.03–0.2 kcal mol^{-1}, and the N-mono is comparably stable or only slightly less stable (by ca. 0.01–0.02 kcal mol^{-1}) than the N-di. The stability of any NgBz isomer also increases in the expected periodic order HeBz < NeBz < ArBz < KrBz < XeBz. The CCSD(T)/CBS BEs range, in particular, between −0.18 and −2.64 kcal mol^{-1} for the N-mono, −0.19 and −2.66 kcal mol^{-1} for the N-di, and −0.23 and −2.82 kcal mol^{-1} for the N-tri, and the values are only slightly lower than those predicted, respectively, for the T_N, T_B and H isomers of the Ng($B_{48}N_{48}H_{24}$) [10]. The CCSD(T)/aVTZ BEs (corrected for the BSSE) of the N-mono, N-di, and N-tri are invariably lower than the CCSD(T)/CBS estimates. This difference is, indeed, not surprising in the light of previous test studies [49] exploring the accuracy of counterpoise-corrected interaction energies compared with CBS estimates. In any case, one notes from Table 3 the nearly coincidence of the CCSD(T)/aVTZ and the (BSSE free) SAPT/aVDZ/mbf BEs.

4.2. Bonding character of the NgBz

The bonding character of the N-tri NgBz (Ng = Ne, Ar, Kr) was recently assayed by an EDA of their HF/aVTZ and MP2/aVTZ electronic energies, and an AIM, NCI, and NBO analysis of their MP2/aVTZ wavefunction [10]. These complexes resulted to be stabilized mainly by the dispersion, its role being by far prevailing over that of the polarization. The AIM and NCI indices were also consistent with this suggestion, and the NBO unraveled only minor charge transfers of 0.0019, 0.0068, and 0.0089 *e* from Ng to Bz. This picture is, however, different from that emerging from the NEDA of the complexes of He, Ne, Ar, and Kr with $B_{12}N_{12}H_{12}$, $B_{27}N_{27}H_{18}$, and $B_{48}N_{48}H_{24}$ [10]. For these systems, in fact, the major attractive term resulted to be the charge transfer, followed by contribution from polarization or from dispersion. The description was substantially similar for the H, T_B, and T_N isomers, and the relative role of the various terms was also nearly independent on Ng. To gain further insights into this issue, we performed the SAPT analysis of the NgBz (Ng = He-Kr). The obtained results, given in Table 4, confirm the dispersive bonding character predicted for the N-tri isomers [10], and unveil a quite similar bonding situation for the N-mono and N-di.

In any NgBz, in fact, the E_{disp} is the by far dominating term, with percentage contributions to the attractive interaction that arrive up to more than 82 % in the HeBz. This percentage progressively decreases in the complexes of the heavier Ng, but still remains close to 70 % in the KrBz. Meanwhile, the role of E_{elst} progressively increases, passing from ca. 12–13 % in the HeBz to ca. 28 % in the KrBz. The percentage contribution of E_{ind} (in SAPT this term includes also the CT) is, instead, only minor (ca. 2–4 %). This description challenges the indication emerged in the recent study [10] of prevailing inductive and charge transfer interactions in the complexes of Ng with BN rings of larger size, and stimulates their re-examination by SAPT or other comparably accurate EDA schemes.

The dispersive character of the NgBz emerged from SAPT is fully consistent with the results of the bonding analysis. The relevant data are given in Fig. 3 and Table 5.

In any NgBz, the $H(\boldsymbol{r}) = 0$ isosurfaces of Ng and Bz (Fig. 3) are perfectly closed, and well separated by a wide region of positive values of $H(\boldsymbol{r})$. The BCPs on the Ng-N bonds are also falling into this region, and the $H(\boldsymbol{r})$ at around the BCPs is positive for a long stretch of the BP. All these contacts are, therefore, assigned as C^l. The numerical indices of these bonds (see Table 5) are also typical of non-covalent contacts, including, in particular, ρ_S(ave) of less than 0.0050 $e\ a_0^{-3}$, and values of $H(\boldsymbol{r})$ that are invariably positive over the probed $s(\boldsymbol{r})$. All the Ng-N bonds are, therefore, assigned as nCov(C^l). Finally, the already noted rather extended shape of the $s(\boldsymbol{r})$ isosurfaces associated with the various BCPs (see Fig. 2) is as well typical of dispersive interactions.

The bonding situation of the NgBz finds a reasonable explanation in the electronic structure of Bz. Thus, as confirmed also by recent high-resolution X-ray diffraction experiments [50], the B_3N_3 ring is only weakly aromatic with an island-like electronic delocalization involving only the N atoms. In essence, the Ng atoms interact with both the B and the N atom(s), but the stability of the NgBz mainly arises from the contact with the electron-rich N, capable of forming decisively intense dispersive contacts. Such contacts do not occur at the electron-poor boron atom(s), also incapable of developing comparably strong bonds of inductive character.

5. Concluding remarks

The calculations performed in this study unveil the dispersive character of the non-covalent bonds occurring between the noble-gas atoms and $B_3N_3H_6$. The interaction may occur by different modes, describable as mono-, di-, and three-coordinated complexes of Ng with the N atom (s), whose stability increases in the order N-mono < N-di < N-tri. Ng interacts indeed with both the B and the N atom(s) of Bz, but the decisively-intense dispersive contacts involve the electron-rich nitrogens. This situation is different from that emerged from a recent DFT study on the interaction of Ng with larger BN sheets such as $B_{12}N_{12}H_{12}$, $B_{27}N_{27}H_{18}$, and $B_{48}N_{48}H_{24}$ [10], whose major binding components were identified as the polarization and charge transfer. These different descriptions invite further investigation. Accurate potentials for Ng interacting with BN sheets are, indeed, also crucial to build accurate PESs for MD simulations of surface processes of technological interest involving noble gases and BN-based surfaces. These simulations will help to highlight the different interaction dynamics for impinging species depending on whether they impact site B or N and will also allow defining the quantities needed for modeling experimental processes, occurring on longer temporal and length scales, such as surface reaction rates and charge exchange.

CRediT authorship contribution statement

Stefano Borocci: Methodology, Data curation, Writing – review & editing. **Armando Camerlingo:** Data curation, Writing – review & editing. **Felice Grandinetti:** Conceptualization, Methodology, Writing – original draft. **Maria Rutigliano:** Writing – review & editing. **Nico Sanna:** Methodology, Software, Writing – review & editing.

Declaration of Competing Interest

The authors declare that they have no known competing financial interests or personal relationships that could have appeared to influence the work reported in this paper.

Data availability

Data will be made available on request.

Acknowledgments

This work was supported by the “Departments of Excellence-2018” Program (Dipartimenti di Eccellenza) of the Italian Ministry of Education, University and Research, DIBAF - Department of University of Tuscia, Project “Landscape 4.0 - food, wellbeing and environment”.

References

[1] D.M. Schubert, Boron advanced materials, Avid. Chem. 1101 (2020) 1–4.
[2] W. Auwärter, Hexagonal boron nitride monolayers on metal supports: Versatile templates for atoms, molecules and nanostructures, Surf. Sci. Rep. 74 (2019) 1–95.
[3] A.C. Levy, T.R. Rybolt, R.A. Pierotti, High-temperature physical adsorption of argon, krypton, and xenon on hexagonal boron nitride, J. Colloid Interface Sci. 70 (1979) 74–82.
[4] P. Shrestha, M.T. Alkhafaji, M.M. Lukowitz, G. Yang, A.D. Migone, Adsorption studies on boron nitride substrates, Langmuir 10 (1994) 3244–3249.
[5] K. Morishige, K. Inoue, K. Imai, X-ray study of Kr, Xe, and N_2 monolayers on boron nitride, Langmuir 12 (1996) 4889–4891.
[6] W. Li, P. Shrestha, A.D. Migone, A. Marmier, C. Girardet, Monolayer Kr films adsorbed on BN, Phys. Rev. B 54 (1996) 8833–8843.
[7] A. Diama, A.D. Migone, Multilayer Kr films adsorbed on BN, Phys. Rev. B 60 (1999) 16103–16108.
[8] H. Dil, J. Lobo-Checa, R. Laskowski, P. Blaha, S. Berner, J. Osterwalder, T. Greber, Surface trapping of atoms and molecules with dipole rings, Science 319 (2008) 1824–1826.
[9] R. Widmer, D. Passerone, T. Mattle, H. Sachdev, O. Gröning, Probing the selectivity of a nanostructured surface by xenon adsorption, Nanoscale 2 (2010) 502–508.
[10] C. John, R.S. Swathi, An anisotropic dressed pairwise potential model for the adsorption of noble gases on boron nitride sheets, Phys. Chem. Chem. Phys. 24 (2022) 2554–2566.
[11] A.D. Becke, Density-functional thermochemistry. III. The role of exact exchange, J. Chem. Phys. 98 (1993) 5648–5652.
[12] C. Lee, W. Yang, R.G. Parr, Development of the Colle-Salvetti correlation-energy formula into a functional of the electron density, Phys. Rev. B 37 (1988) 785.
[13] E.D. Glendening, Natural energy decomposition analysis: Explicit evaluation of electrostatic and polarization effects with application to aqueous clusters of alkali metal cations and neutrals, J. Am. Chem. Soc. 118 (1996) 2473–2482.
[14] M. Wen, Z.Z. Li, A.Y. Li, Noble gas inserted compounds of borazine and its derivative $B_3N_3R_6$: structures and bonding, J. Mol. Model. 24 (2018) 1–13.
[15] A. Boshra, A.R. Oliaey, F. Rezaie, Y. Bazvand, S.B.A. Hamid, Novel cations of xenon trifluoroborazine complexes: Structures, reactivities, and natural bonding orbital analysis, J. Fluor. Chem. 178 (2015) 99–106.
[16] S.P. Kuntar, A. Ghosh, T.K. Ghanty, Superstrong chemical bonding of noble gases with oxidoboron (BO+) and sulfidoboron (BS+), Chem. - Eur. J. 126 (2022) 7888–7900.
[17] S. Bavafa, A. Nowroozi, A. Ebrahimi, Ab initio study of aerogen-bonds between some heterocyclic compounds of benzene with the noble gas elements (Ne, Ar, and Kr), Struct. Chem. 31 (2020) 435–445.
[18] C. Møller, M.S. Plesset, Note on an approximation treatment for many-electron systems, Phys. Rev. 46 (1934) 618–622.
[19] T. Lu, F. Chen, Multiwfn: a multifunctional wavefunction analyzer, J. Comput. Chem. 33 (2012) 580–592.
[20] T. Lu, Q. Chen, Simple, efficient, and universal energy decomposition analysis method based on dispersion-corrected density functional theory, J. Phys. Chem. A 7023-7035.
[21] J.S. Murray, P. Politzer, The electrostatic potential: an overview, WIREs Comput. Mol. Sci. 1 (2011) 153–163.
[22] A. Yadav, S.S. Dindorkar, Adsorption behaviour of hexagonal boron nitride nanosheets towards cationic, anionic and neutral dyes: insights from first principle studies, Colloids Surf. A 640 (2022), 128509.
[23] F. Grandinetti, Noble gas chemistry: structure, bonding, and gas-phase chemistry, John Wiley & Sons, 2018.
[24] S. Borocci, F. Grandinetti, N. Sanna, Complexes of $NgHNg^+$ (Ng = He, Ne, Ar) with He: theoretical insights into structure, stability, and bonding character, Chem. Phys. Lett. 819 (2023), 140443.
[25] B. Jeziorski, R. Moszyński, K. Szalewicz, Perturbation theory approach to intermolecular potential energy surfaces of van der Waals complexes, Chem. Rev. 94 (1994) 1887–1930.
[26] S. Borocci, M. Giordani, F. Grandinetti, Bonding motifs of noble-gas compounds as described by the local electron energy density, J. Phys. Chem. A 119 (2015) 6528–6541.
[27] S. Borocci, F. Grandinetti, N. Sanna, F. Nunzi, Classifying the chemical bonds involving the noble-gas atoms, New J. Chem. 44 (2020) 14536–14550.
[28] S. Borocci, F. Grandinetti, N. Sanna, Noble gas compounds: A general procedure of bonding analysis, J. Chem. Phys. 156 (2022), 014104.
[29] M. Rutigliano, P. Gamallo, R. Sayós, S. Orlandini, M. Cacciatore, A molecular dynamics simulation of hydrogen atoms collisions on an H-preadsorbed silica surface, Plasma Sources Sci. Technol. 23 (2014), 045016.
[30] D. Bruno, M. Cacciatore, S. Longo, M. Rutigliano, Gas-surface scattering models for particle fluid dynamics: a comparison between analytical approximate models and molecular dynamics calculations, Chem. Phys. Lett. 320 (2000) 245–254.
[31] S. Boccelli, T.E. Magin, A. Frezzotti, Numerical investigation of reversed gas feed configurations for Hall thrusters, J. Propul. Power 37 (2021) 919–927.
[32] M. Iannuzzi, Ar Implantation at the hBN/Rh(111) nanomesh by ab Initio molecular dynamics, J. Phys. Chem. C 119 (2015) 22198–22207.
[33] M.W. Crofton, J.A. Young, Low energy Xe+ sputter yields for alumina, Hiperco 50, and boron nitride, AIP Adv. 11 (2021), 125126.
[34] R.F.W. Bader, Atoms in Molecules: a Quantum Theory, Oxford University Press, Oxford, 1990.
[35] D. Cremer, E. Kraka, Chemical bonds without bonding electron density - does the difference electron-density analysis suffice for a description of the chemical bond? Angew. Chem. Int. Ed. Engl. 23 (1984) 627–628.
[36] D. Cremer, E. Kraka, A description of the chemical bond in terms of local properties of electron density and energy, Croat. Chem. Acta 57 (1984) 1259–1281.
[37] E.R. Johnson, S. Keinan, P. Mori-Sanchez, J. Contreras-Garcia, A.J. Cohen, W. Yang, Revealing noncovalent interactions, J. Am. Chem. Soc. 132 (2010) 6498–6506.
[38] C. Narth, Z. Maroun, R.A. Boto, R. Chaudret, M.L. Bonnet, J.-P. Piquemal, J. Contreras-García, A complete NCI perspective: from new bonds to reactivity, in: Applications of Topological Methods in Molecular Chemistry, Springer, Cham, 2016, pp. 491–527.
[39] K. Raghavachari, G.W. Trucks, J.A. Pople, M. Head-Gordon, A fifth-order perturbation comparison of electron correlation theories, Chem. Phys. Lett. 157 (1989) 479–483.
[40] B.P. Pritchard, D. Altarawy, B. Didier, T.D. Gibson, T.L. Windus, New basis set exchange: an open, up-to-date resource for the molecular sciences community, J. Chem. Inf. Model. 59 (2019) 4814–4820. https://www.basissetexchange.org.
[41] K.A. Peterson, D. Figgen, E. Goll, H. Stoll, M. Dolg, Systematically convergent basis sets with relativistic pseudopotentials. II. Small-core pseudopotentials and correlation consistent basis sets for the post-*d* Group 16–18 elements, J. Chem. Phys. 119 (2003) 11113–11123.

[42] S.F. Boys, F. Bernardi, The calculation of small molecular interactions by the differences of separate total energies. Some procedures with reduced errors, Mol. Phys. 19 (1970) 553–566.
[43] A. Halkier, T. Helgaker, P. Jørgensen, W. Klopper, H. Koch, J. Olsen, A.K. Wilson, Basis-set convergence in correlated calculations on Ne, N_2, and H_2O, Chem. Phys. Lett. 286 (1998) 243–252.
[44] M.J. Frisch, G.W. Trucks, H.B. Schlegel, G.E. Scuseria, M.A. Robb, J.R. Cheeseman, G. Scalmani, V. Barone, B. Mennucci, G.A. Petersson, et al., Gaussian09, Revision D.01, Gaussian Inc., Wallingford CT, 2013.
[45] R. Bukowski, W. Cencek, P. Jankowski, M. Jeziorska, B. Jeziorski, S.A. Kucharski, V.F. Lotrich, M.P. Metz, A.J. Misquitta, R. Moszyński, K. Patkowski, R. Podeszwa, F. Rob, S. Rybak, K. Szalewicz, H.L. Williams, R.J. Wheatley, P.E.S. Wormer, P.S. Żuchowski, SAPT2016: An ab initio program for symmetry-adapted perturbation theory calculations of intermolecular interactions energies. Sequential and parallel versions, University of Delaware and University of Warsaw, 2016.
[46] F.-M. Tao, Y.-K. Pan, *Ab initio* potential energy curves and binding energies of Ar_2 and Mg_2, Mol. Phys. 81 (1994) 507–518.
[47] G. Saleh, C. Gatti, L. Lo Presti, Energetics of non-covalent interactions from electron and energy density distributions, Comput. Theor. Chem. 1053 (2015) 53–59.
[48] T. Weber, E. Riedle, H.J. Neusser, E.W. Schlag, Van der Waals bond lengths and electronic spectral shifts of the benzene-Kr and benzene-Xe complexes, Chem. Phys. Lett. 183 (1991) 77–83.
[49] J.R. Alvarez-Idaboy, A. Galano, Counterpoise corrected interaction energies are not systematically better than uncorrected ones: comparison with CCSD(T)/CBS extrapolated values, Theor. Chem. Acc. 126 (2010) 75–85.
[50] M.D.R. Merino-García, L.A. Soriano-Agueda, J.D.D. Guzmán-Hernández, D. Martínez-Otero, B. Landeros Rivera, F. Cortés-Guzmán, J.E. Barquera-Lozada, V. Jancik, Benzene and borazine, so different, yet so similar: insight from experimental charge density analysis, Inorg. Chem. 61 (2022) 6785–6798.